

# Numerical modeling and performance of continuous thermally regenerative electrochemical cycle

Yixuan Li <sup>1</sup>, Weicong Xu <sup>1\*</sup>, Li Zhao <sup>1</sup>

<sup>1</sup> Tianjin University, Tianjin 300350, China

(\*Corresponding Author: xuweicong@tju.edu.cn)

## ABSTRACT

Recycling low and medium heat is important for saving energy and reducing pollutant emissions. The continuous thermally regenerative electrochemical cycle (C-TREC) have attracted attention because of their ability to continuously output electrical energy. In this study, a two-dimensional stationary model coupling flow and electrochemical reactions is developed to investigate the flow and C-TREC electrochemical reactions during the charging and discharging process of a continuous thermally regenerative electrochemical cycle. The effects of porous electrode geometry, porosity, current density, overpotential, and temperature difference between hot and cold sources on the performance of C-TREC are analyzed. The study specifies the operation strategy during charging and discharging.

**Keywords:** low and medium temperature thermal energy, thermally regenerative electrochemical cycle, charge-discharge process

## NONMENCLATURE

### Abbreviations

C-TREC continuous thermally regenerative electrochemical cycle

### Symbols

c	Concentration (mol m <sup>-3</sup> )
cp	specific heat (J kg <sup>-1</sup> K <sup>-1</sup> )
D	Diffusion coefficient (m <sup>2</sup> s <sup>-1</sup> )
df	Fiber diameter (m)
E	Electromotive force (V)
F	Faraday constant (96485C mol <sup>-1</sup> )
j <sub>0</sub>	exchange current density (A m <sup>-2</sup> )
k <sub>0</sub>	reaction rate constant (m s <sup>-1</sup> )
n	number of electrons transferred
P	power density (W m <sup>-2</sup> )
Q	heat load (W)
T	temperature (K)
z	ion valence
v	flow velocity (m s <sup>-1</sup> )

## 1. INTRODUCTION

Low-grade thermal energy is widely available in various sources such as solar energy, geothermal energy, vehicles, and industrial waste heat. According to a study, waste heat below 230 °C accounts for approximately 60% of the total waste heat. [1] This vast amount of low-grade thermal energy presents significant potential for recycling and reuse on a global scale.

Conventional thermal cycles such as the organic Rankine cycle and the Stirling cycle that realize heat power conversion have been widely studied for more than a decade [2]. However, there are still problems such as high system complexity and limited efficiency improvement [3]. Hence, the development of an efficient thermal energy recovery system is crucial for the effective utilization of low-grade thermal energy.

In the recent decade, scholars have proposed a novel approach to convert low-grade thermal energy into electrical energy through thermo-electrochemical methods, which follows the energy conversion path of "thermal energy-Gibbs free energy transformation-electrical work", can convert low and medium temperature thermal energy into electrical energy. This type of system possesses characteristics such as a simple system structure, lightweight devices, and the use of environmentally friendly materials. It is anticipated to evolve into a new generation of large-scale low-grade thermal energy recycling technology. For low-grade thermal energy at temperatures lower than 100°C, liquid-based thermo-electrochemical systems show excellent thermoelectric conversion efficiency [4].

Liquid-based thermo-electrochemical systems include: Thermally regenerative electrochemical cycle (TREC) [5], Thermally-regenerative flow battery (TRFB) [6], Thermo-electrochemical cell (TEC) [7], Thermally regenerative ammonia-based battery (TRAB) [8], Thermo-osmotic energy conversion (TOEC) [9]. Among these approaches, TREC utilizes the reversible potential change of electrode reactions with temperature. This enables the system to be charged and discharged at

different temperatures, thereby achieving the conversion of thermal energy into electrical energy [10], and the output of net electrical work is realized by the voltage difference between charging and discharging, thus completing the conversion of thermal energy to electrical energy.

In TREC systems with a positive temperature coefficient, the discharging process takes place at high temperatures, while the charging process occurs at low temperatures. The opposite is true for TREC with a negative temperature coefficient [11]. Figure 1 shows the corresponding T-S diagram. For a system with a positive temperature coefficient, there are four specific processes, which are heating, discharging, cooling, and charging processes. The heating process heats the battery to a high temperature (TH) in the open-circuit state; the discharge process discharges the battery externally at a high temperature; the cooling process cools the battery to a low temperature (TL) in the open-circuit state; and the charging process charges the battery at a low temperature. The net work obtained is represented in the temperature-entropy diagram as the area enclosed by the cycle.

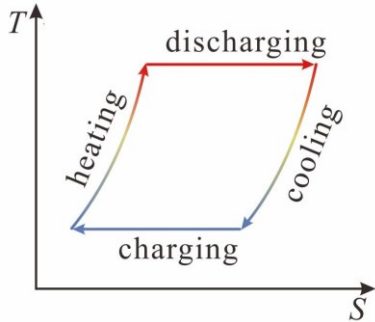


Fig. 1 Temperature-entropy diagram of continuous TREC system

According to the continuity of operation, TREC can be divided into intermittent and continuous TREC. However, the utilization scenarios of intermittent TRECs are limited by the fact that the power output cannot be sustained due to the inability to cycle the battery device. To solve these problems, Poletayev [12] proposed a C-TREC by combining a thermo-electrochemical system with a liquid flow battery.

A schematic diagram of the system structure of the continuous TREC is given in Figure 2. C-TREC system consists of two electrochemical reaction cells, two heat exchangers, two peristaltic pumps, piping and an external load. The two electrochemical reaction cells operate at different temperatures, with one cell charging and the other discharging, and the electrolyte is circulated between the two cells by means of a peristaltic pump. The continuous TREC has no need for an external

auxiliary power supply since the discharging cell can supply power to the charging cell through an external circuit. A heat exchanger is used to transfer heat and preheat or pre-cool the regenerating electrolyte, which effectively improves the overall system efficiency. To ensure continuous operation under ideal conditions, the redox substances are present only in the electrolyte, while the electrodes solely act as carriers for electron transfer without direct participation in the redox reaction.

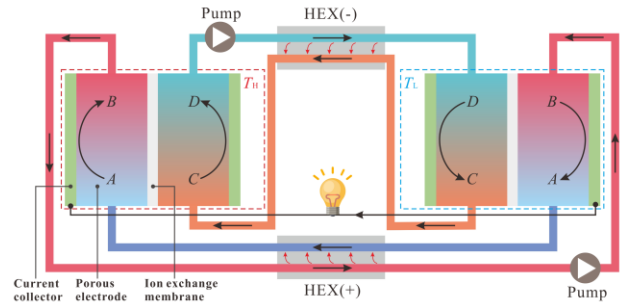


Fig. 2 Schematic of the C-TREC system

Existing studies on TRECs mainly focus on intermittent TRECs, which can achieve a high degree of thermodynamic refinement by choosing suitable electrolyte and electrode materials because the electrolyte and electrodes can participate in the redox reaction at the same time. Gao et al [13] achieved the highest thermodynamic perfection of 50% for intermittent TREC using  $\text{RbNO}_3 + \text{Cu}(\text{NO}_3)_2$  as electrolyte and  $\text{CuHCFe@Rb/Cu}$  as electrode. In comparison, there are fewer studies on continuous TREC. Due to the electrodes not participating in the reaction, this kind of system is usually based on porous carbon materials as electrodes. Poletayev et al [8] established a continuous TREC with  $\text{V}^{2+}/\text{V}^{3+}$  and  $\text{Fe}(\text{CN})_6^{3-}/\text{Fe}(\text{CN})_6^{4-}$  as redox couples, which can effectively recover the low-temperature waste heat, but its main purpose is to improve the energy storage performance of the liquid-flow battery rather than to realize thermoelectric conversion. Zhang et al [10] used  $\text{Fe}(\text{CN})_6^{3-}/\text{Fe}(\text{CN})_6^{4-}/\text{KCl}$  as electrolytes and  $\text{Ni}_0.2\text{Co}_0.8(\text{OH})_2/\text{Zn}$  as electrodes for cycling at temperatures ranging from 25-55 °C, and achieved a thermoelectric conversion efficiency of 3.61%. Reynard and Eapen [11,12] connected a vanadium redox flow battery with a TREC for coupling, which improved the system efficiency and cycling performance. Ding et al [13] proposed a continuous TREC with  $\text{Fe}(\text{CN})_6^{3-}/\text{Fe}(\text{CN})_6^{4-}$  and  $\text{I}_3^-/\text{I}^-$  as the electrolyte, which achieved a thermodynamic perfection of 12%. Qian et al [14] used  $\text{Fe}(\text{CN})_6^{3-}/\text{Fe}(\text{CN})_6^{4-}$  and  $\text{I}_3^-/\text{I}^-$  as the electrolyte for the continuous TREC, which effectively solved the mismatch of the pH between

anodic and cathodic electrolytes resulting in unstable system operation. Bleeker et al [15] improved the temperature coefficient of the liquid-flow battery to 2.88 mV K<sup>-1</sup> by changing the electrolyte concentration, using the same electrolyte as in Qian's article and using KCl as the supporting electrolyte, but the thermal efficiency was only 0.004% due to the heat exchanger and the internal resistance. Li et al [16] established a continuous

TREC using the CuHCF as cathode and Cu/Cu<sup>2+</sup> as anode in a continuous TREC experimental system, and the thermal

efficiency reached 1.76%. Chen et al [17] constructed a two-dimensional model of coupled flow and electrochemical fields, and the thermal efficiency could reach 8.3%. The related literature research is summarized in Table 1.

Table 1 Summary of current research on C-TREC

Year	Authors	Electrolytes	Electrodes	T <sub>H</sub> -T <sub>L</sub> (°C)	α	η <sub>th</sub> (%)	Research Methods
2018	Poletayev et al.[8]	V <sup>2+/3+</sup> / Fe(CN) <sub>6</sub> <sup>3-/4-</sup>	Carbon	0-50	3	1.86	experiment
2018	Reynard et al.[11]	V <sup>5+/4+</sup> / V <sup>3+/2+</sup>	Carbon	20-60	1.16	0.92	experiment
2019	Ding et. al.[13]	Fe(CN) <sub>6</sub> <sup>3-/4-</sup> , I <sup>-</sup> /I <sub>3</sub> <sup>-</sup>	Solid electrodes	30-65	1.8	0.37	experiment
2019	Eapen et al.[12]	V <sup>5+/4+</sup> / V <sup>3+/2+</sup>	Carbon	30-60	-	0.50	experiment
2021	Zhang et al.[10]	Fe(CN) <sub>6</sub> <sup>3-/4-</sup> , KCl	Ni <sub>0.2</sub> Co <sub>0.8</sub> (OH) <sub>2</sub> /Zn	25-55	1.46	3.61	experiment
2021	Qian et.al.[14]	Fe(CN) <sub>6</sub> <sup>3-/4-</sup> , I <sup>-</sup> /I <sub>3</sub> <sup>-</sup>	Carbon	23-60	1.9	0.1	experiment
2021	Bleeker et.al.[15]	Fe(CN) <sub>6</sub> <sup>3-/4-</sup> , I <sup>-</sup> /I <sub>3</sub> <sup>-</sup>	Carbon felt	20-54	2.88	0.004	experiment & simulation
2022	Li et.al.[17]	RbNO <sub>3</sub> , Cu(NO <sub>3</sub> ) <sub>2</sub>	Carbon	10-50	1.76	1.76	experiment
2022	Chen et.al[16]	Fe(CN) <sub>6</sub> <sup>3-/4-</sup> , I <sup>-</sup> /I <sub>3</sub> <sup>-</sup>	Carbon	23-60	8.3	8.3	simulation

The literature summary reveals that experimental methods are predominantly used to study C-TRECs, while numerical simulation research in this area is relatively scarce. Therefore, there is a need to establish a numerical model that facilitates rapid calculations aligned with engineering applications. In practical applications, the performance of electrochemical reaction cells is affected by many factors, and the computational results of the model can give information that is difficult to be measured by conventional experiments, such as the electrolyte ion concentration field inside the cell, the distribution of the electric field, and the change of the electric potential. Therefore a numerical model is needed to reveal the parameter changes of the electrochemical reaction process.

## 2. MODELING

### 2.1 Geometric Model

When an electrolyte passes through a porous electrode, the active substance within it diffuses towards the electrode's surface, where it undergoes an electrochemical reaction. As this reaction takes place, the concentration of the active substance varies in the direction perpendicular to the electrode, also known as the Y direction. Consider a general electrode reaction:



In this context, Ox represents the oxidizing species, while Red represents the reducing species in the redox reaction. n denotes the number of electrons transferred in the reaction, and v represents the stoichiometric coefficient of each participating species, indicating the molar ratio of each substance involved in the reaction.

The equations are solved in the software COMSOL Multiphysics 6.1, which is suitable for solving problems with multiple coupled physical fields. Since the effect of electrolyte concentration change on the flow field is neglected and the flow and electrochemical fields are unidirectionally coupled, the electrolyte flow is mainly considered to affect the electrode reaction through mass transport.

The flow of electrolyte in porous electrodes is simulated by using the Brinkman equation toolbox in the software, and the direct linear solver is PARDISO with a relative error configuration of 10<sup>-3</sup>. A cubic current distribution is used for both the positive and negative electrode sides, and a quadratic current distribution is used for the membrane side.

Fig. 3 shows the continuous TREC 2D geometric model and detailed mesh distribution. The flow of electrolyte occurs in the X-Y plane of the model and the geometric model consists of three domains: a negative porous electrode, a ion exchange membrane, and a positive porous electrode. The model incorporates the

interaction of flow and electrochemical fields, where each species is transported through various mechanisms such as diffusion, electromigration, and convection. All species involved in electrochemical reactions adhere to the principles of mass, charge, and momentum conservation. The following assumptions were proposed in this study:

(1)The electrolyte is considered an incompressible fluid with laminar inflow.

(2)The electrolyte is a dilute, electrically neutral solution.

(3)It is assumed that all domains are under isothermal conditions, and the physical properties of the electrodes, electrolyte, and membrane are assumed to be isotropic and homogeneous.

(4)The viscosity of the electrolyte does not vary as the concentrations continuously change with the progress of electrode reactions.

(5)Neglect the effect of gravity.

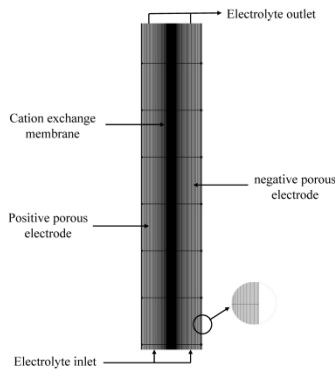


Fig. 3 Mesh distribution of 2D geometry model

## 2.2 Physical model

### 2.2.1 Control equations for electrolyte flow

The flow of electrolyte in porous electrodes is governed by the incompressible fluid Navier-Stokes equation and the continuous Blackman equation [22]:

$$\rho(u \cdot \nabla)u = -\nabla p + \mu \nabla^2 u \quad (2)$$

$$\nabla u = 0 \quad (3)$$

where  $u$  is the linear velocity of the electrolyte, [m/s];  $p$  is the pressure of the electrolyte, [Pa];  $\rho$  is the density of the electrolyte, [kg/m<sup>3</sup>]; and  $\mu$  is the kinetic viscosity, [Pa·s].  $\rho$  and  $\mu$  are taken as constants.

$K$  is the permeability of the porous electrode which can be solved by the Kozeny-Carman equation:

$$K = d_f^2 \varepsilon^3 / 16 K_c (1 - \varepsilon)^2 \quad (4)$$

where  $d_f$  is the fiber diameter [mm] and  $K_c$  is the Carman-Kozeny constant.

### 2.2.2 Conservation equations for mass transport

During the flow of the electrolyte, the substance transport of each substance  $i$  is controlled by the Nernst-Planck equation:

$$N_i = -D_i \nabla c_i - \left( \frac{z_i c_i D_i F}{RT} \right) \nabla \phi + c_i u \quad (5)$$

where  $c_i$  represents the concentration of species  $i$  in the electrolyte, [M]; where  $N_i$  is the flux of species  $i$ , [mol/(m<sup>2</sup>·s)];  $D_i$  (see Table 2), [m<sup>2</sup>/s], and  $z_i$  are the diffusion coefficient and the valence, respectively;  $\phi$  is the ionic potential within the electrolyte, [V];  $T$  is the temperature of the electrolyte, [K]; and  $F$  and  $R$  are the Faraday constant and the gas constant.

$D_i^{eff}$  is obtained from the Bruggemann correction equation:

$$D_i^{eff} = \varepsilon^{3/2} D_i \quad (6)$$

$\varepsilon$  is the porosity of the porous electrode.

The electrolyte needs to satisfy electrically neutral conditions [23]:

$$\sum_i z_i c_i = 0 \quad (7)$$

In the steady state model, where the concentration of a substance  $c_i$  does not vary with time, there is:

$$\nabla N_i = 0 \quad (8)$$

### 2.2.3 Conservation equations for charge

According to the definition of current density, the total current density in the electrolyte is:

$$j_e = F \sum_i z_i N_i = -k \nabla - F \sum_i z_i D_i \nabla c_i \quad (9)$$

In Eq. (9), the electrolyte conductivity  $k$  is defined as:

$$k = \frac{F^2}{RT} \sum_i z_i^2 D_i c_i \quad (10)$$

The total current is controlled by the current continuity equation:

$$\nabla j_e + \frac{\partial \rho}{\partial t} = Q \quad (11)$$

Where  $\rho$  is the charge density of the electrolyte, [C/m<sup>3</sup>]. In the steady state model, the charge density does not change with time,  $Q$  is the current source term, there is no chemical reaction at the electrolyte,  $Q=0$  therefore there is:

$$\nabla j = 0 \quad (12)$$

In the cation exchange membrane, a secondary current distribution is used, and the concentration of each substance is uniformly distributed, so the current density in the membrane is:

$$j_e = -k_m \nabla \phi \quad (13)$$

where  $k_m$  represents the electrolyte conductivity in the membrane, [S/m], considered as a constant.

### 2.3 Boundary condition

The electrolyte enters the porous electrode as a laminar flow at a prescribed average velocity  $u_{in}$  (in the y-direction), with a constant concentration of each electrolyte  $c_i = c_i^0$ . The average velocity at the inlet is obtained from the volumetric flux:

$$u_{in} = Q_v / 60wd \quad (14)$$

where  $Q_v$  is the volumetric flow rate, [m<sup>3</sup>/s];  $w$  is the porous electrode width, [mm]; and  $d$  is the length of the porous electrode in the z direction, [mm].

A redox reaction occurs on the surface of the positive and negative electrodes and the current density is given by the Butler-Volmer equation:

$$j = j_0 \left[ \frac{C_o^s}{C_o} e^{(\alpha)F\eta/(RT)} - \frac{C_R^s}{C_R} e^{-(1-\alpha)F\eta/(RT)} \right] \quad (15)$$

where  $j$  is the local current density, [mA/mm<sup>2</sup>], the superscript  $s$  is the surface,  $\alpha$  and  $1-\alpha$  are the transfer coefficients in the reduction and oxidation directions, respectively;  $n$  is the number of electrons involved in the reaction;  $\eta$  is the reaction overpotential, [V], the difference between the electrode potential at which the electrode reaction departs from equilibrium and the equilibrium potential for this electrode reaction; and  $j_0$  is the exchange current density, which is related to the reaction rate constant,  $k_0$ , and is defined by the exchange current density  $j_0$ :

$$j_0 = nFk_0C_o^{1-\nu_o\alpha_o}C_R^{\nu_R\alpha_R} \quad (16)$$

The overpotential is expressed as:

$$\eta = \phi_s - \phi_e - E_{eq} \quad (17)$$

$\phi_s, \phi_e$  represent electrolyte potential and electrode potential, [V], respectively;  $E_{eq}$  denotes equilibrium potential, [V]; which can be obtained from the Nernst equation:

$$E_{eq} = E^{0'} + \frac{RT}{nF} \ln \frac{C_o^{\nu_o}}{C_R^{\nu_R}} \quad (18)$$

where  $E^{0'}$  is the standard potential at temperature  $T$ .

The potential at the boundary between the electrolyte and the membrane is continuous:

$$\phi_{+,m} = \phi_+ \quad (19)$$

$$\phi_{-,m} = \phi_- \quad (20)$$

Taking into account the difference in electrode surface potentials, the average integration method is used to solve for the single cell voltage:

$$E_{cell} = \frac{1}{h} \int_0^h [\phi_{+,s}(x) - \phi_{-,s}(x)] dx \quad (21)$$

Temperature of heat sink ( $T_L$ )	25°C
Concentration of $I^-$ ( $c_{I^-}^0$ )	1M
Concentration of $I_3^-$ ( $c_{I_3^-}^0$ )	0.1M
Concentration of $Fe(CN)_6^{3-}$ ( $c_{Fe(CN)_6^{3-}}^0$ )	0.375M
Concentration of $Fe(CN)_6^{4-}$ , ( $c_{Fe(CN)_6^{4-}}^0$ )	0.375M
Electrolyte flow velocity ( $v$ )	0.5–200 $\mu\text{m s}^{-1}$
Diffusivity of $KI_3$ ( $D_{O,+}$ )	$7.0 \times 10^{-10} \text{ m}^2/\text{s}$
Diffusivity of $KI$ ( $D_{O,-}$ )	$5.4 \times 10^{-10} \text{ m}^2/\text{s}$
Diffusivity of $K_3Fe(CN)_6$ ( $D_{R,-}$ )	$7.6 \times 10^{-10} \text{ m}^2/\text{s}$
Diffusivity of $K_4Fe(CN)_6$ ( $D_{O,-}$ )	$6.9 \times 10^{-10} \text{ m}^2/\text{s}$
Rate constant of $I_3^-/I^-$ ( $k_c$ )	$6.7 \times 10^{-5} \text{ m s}^{-1}$
Rate constant of $Fe(CN)_6^{3-/4-}$ ( $k_R$ )	$7.5 \times 10^{-6} \text{ m s}^{-1}$
Negative equilibrium potential, $E_{o^1}$	0.536V
Positive equilibrium potential, $E_{o^2}$	0.37V

### 2.4 Performance Evaluation Model

The voltage of a C-TREC system is determined by the voltage difference between the cells at the hot and cold ends:

$$\Phi = E_H - E_L \quad (22)$$

The voltage of the C-TREC system is determined by the voltage difference between the high and low temperature cells:

$$P = \Phi \cdot I \quad (23)$$

where  $I$  is the electrode current density.

The thermoelectric conversion efficiency equation is:

$$\eta_e = \frac{P - W_p}{Q_s + Q_r} \quad (24)$$

where  $W_p$  is the pump work,  $Q_s$  is the heat load required to heat the electrolyte from  $T_L$  to  $T_H$ , and  $Q_r$  is the heat load during the electrochemical reaction.

Therefore the thermoelectric conversion efficiency equation is:

$$\eta_e = \frac{P}{(1 - \eta_H)\Delta T \sum_i \rho_i c_{p,i} Q_{v,i}} \quad (25)$$

## 3. DISCUSSION

### 3.1 Model validation

In order to validate the model, the results obtained from the model are compared with published experimental results. Fig. 4(a), (b) shows the results of the validation of the model with experimental work conducted by Qian et al. [24], where solid lines and circles correspond to electrolyte flow rates of 230  $\mu\text{L min}^{-1}$  and 340  $\mu\text{L min}^{-1}$ , respectively, and dashed lines and squares correspond to electrolyte flow rates of 62  $\mu\text{L min}^{-1}$  and 149  $\mu\text{L min}^{-1}$ . It can be observed from Fig. 4, the model matches well with the experimental data, and the maximum error of power density is only 5.1%, which

Table 2 Operational parameters for modeling

Parameters	Values
Temperature of heat source ( $T_H$ )	60°C

verifies the correctness of the model. At four flow rates, the voltage varies almost linearly with the circulating current density, and at larger flow rates, the simulated power density values deviate from the experiments, and the deviation of the power density increases gradually with the increase of the electrolyte flow rate, and the flow rate of all the electrolytes in this study is lower than  $600 \mu\text{L min}^{-1}$ , and this model is a steady-state model, and the errors observed in this range are kept within a reasonable range.

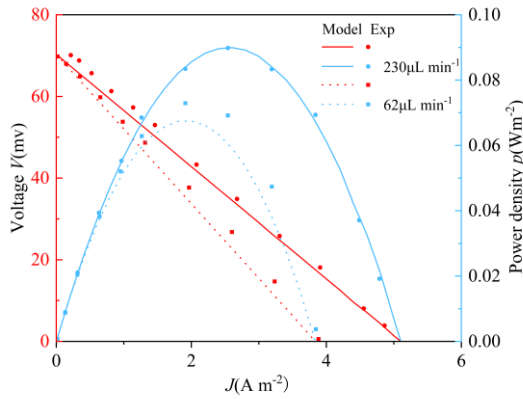


Fig. 4 (a) Comparison of experimental and simulated results of power density against voltage under  $62 \mu\text{L min}^{-1}$  and  $230 \mu\text{L min}^{-1}$  electrolyte flow rates

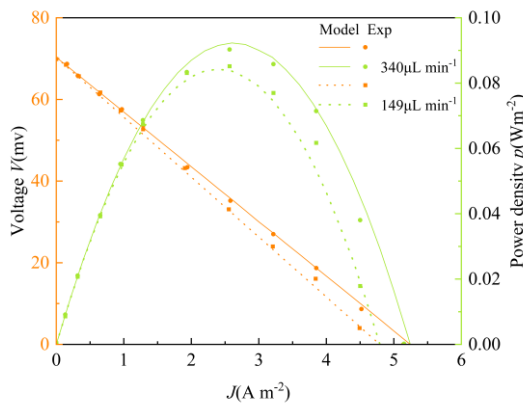


Fig. 4 (b) Comparison of experimental and simulated results of power density against voltage under  $149 \mu\text{L min}^{-1}$  and  $340 \mu\text{L min}^{-1}$  electrolyte flow rates

### 3.2 Influence of porous electrode geometry and porosity

The geometry of the electrodes may directly affect the distribution of the electrolyte, and thus have an effect on the performance of a C-TREC system. Fig. 5(a) shows the plot of power density versus voltage at electrode thicknesses of 1.5 mm, 2.5 mm, and 3.5 mm. It can be observed from the figure that the decrease in electrode thickness leads to an increase in the voltage

and maximum power density of the system. The system voltage and maximum power density were maximized when the electrode thickness was 1.5 mm, which was attributed to the fact that decreasing the thickness of the porous electrode accelerates the flow rate of the electrolyte inside the electrode under the same volumetric flux condition, thus enhancing the mass transfer effect.

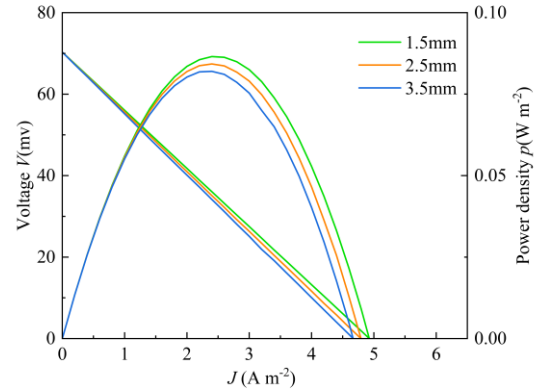


Fig. 5(a) Effect of different electrode thickness on system performance

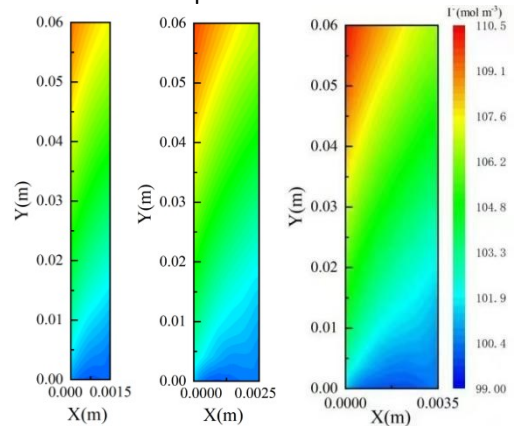


Fig. 5(b) Distribution of  $\text{I}^-$  concentration at different electrode thicknesses when the current density is  $-3 \text{ A m}^{-2}$

Electrode porosity is one of the important elements to influence the performance of a continuous TREC system. Porosity is a parameter that describes the ratio between the pore volume and the total volume in a porous electrode, and different porosities will have different effects on the performance of the cell. From equation (6), the porosity affects the effective conductivity of the electrode and the effective diffusion coefficient of ions in the electrode, and the electrode porosity affects the distribution of the flow field. The relationship between power density and voltage at 0.65, 0.75, 0.85, and 0.95 porosity is given in Fig. 6.

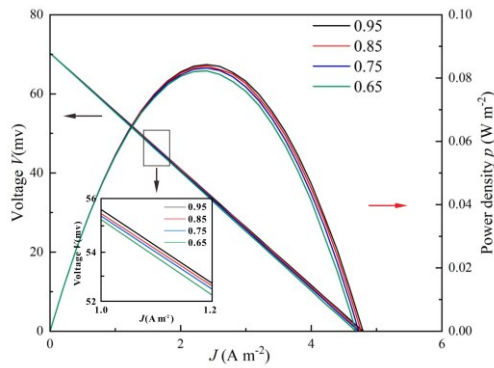


Fig. 6 Variation of voltage and power density of the system with different electrode porosities

### 3.3 Influence of current density

The variation of current density has a significant effect on the performance of the C-TREC system. In order to investigate the effect of different current densities on the performance of the system, the concentration distribution of  $I^{3-}$  in the anodic porous electrode was investigated at current densities of -1, -3, and -5  $A\ m^{-2}$  and a flow rate of  $149\ \mu L\ min^{-1}$  in a cell at  $60\ ^\circ C$ , for example. As Figure 7 shows, when the current density was increased from  $-1\ A\ m^{-2}$  to  $-5\ A\ m^{-2}$ , it was clearly observed that the concentration distribution of  $I^-$  became inhomogeneous and a large concentration gradient was formed. This is because with increasing current density inside the electrode, the rate of charge transfer is accelerated, thus increasing the rate of electrochemical reactions, but it also leads to an increase in overpotential. Hence, as the current density increases, the power density of the system experiences an initial rise and then a gradual decline.

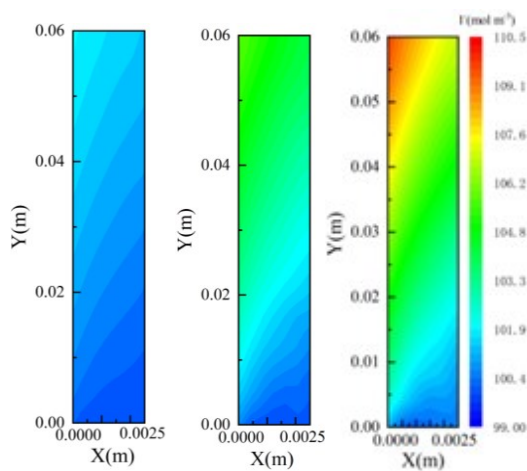


Fig. 7 Concentration distribution field of  $I^-$  in the anode at current densities of  $-1\ A\ m^{-2}$ ,  $-3\ A\ m^{-2}$  and  $-5\ A\ m^{-2}$  when the cell temperature is  $60\ ^\circ C$

### 3.4 Effects of overpotential distribution

Overpotential is an important parameter affecting mass transfer in C-TREC systems. Figures 8(a)-(c) represent the distribution of overpotentials within the positive and negative electrodes when the flow rates were  $62$ ,  $149$ , and  $340\ \mu L\ min^{-1}$  at  $60\ ^\circ C$  and a current density of  $-4\ A\ m^{-2}$ . The results indicate that the overpotential distribution trends of the two electrodes are similar, and the higher the electrolyte flow rate, the smaller the overpotential and inhomogeneity inside the cell, which indicates that the higher the electrolyte flow rate, the more uniform the electrolyte distribution, the better the mass transfer performance, and the better the overall performance of the cell. When the electrolyte flow rate increases, the redox reaction rate is accelerated, and the mass transfer rate then becomes faster and faster.

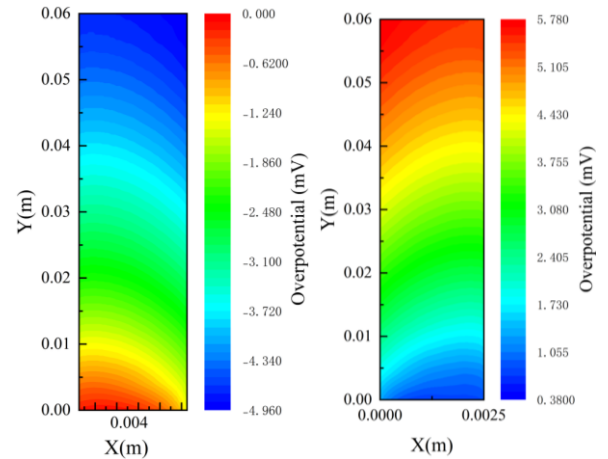


Fig.8 (a) Negative and positive overpotential distribution when the flow rate is  $62\ \mu L\ min^{-1}$  and the current is  $-4\ A\ m^{-2}$  overpotential distribution

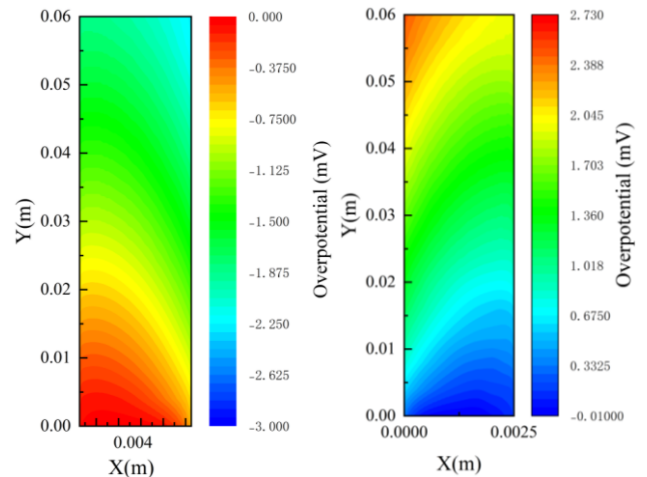


Fig.8 (b) Negative and positive overpotential distribution when the flow rate is  $149\ \mu L\ min^{-1}$  and the current is  $-4\ A\ m^{-2}$  overpotential distribution

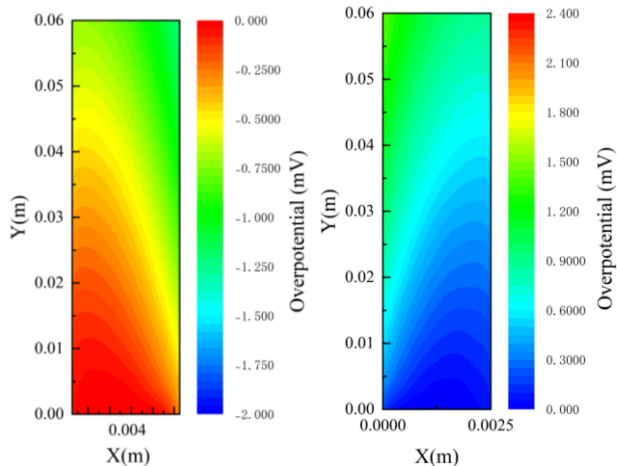


Fig.8 (c) Negative and positive and negative overpotential distribution when the flow rate is  $340\mu\text{L min}^{-1}$  and the current is  $-4\text{ A m}^{-2}$  overpotential distribution

### 3.5 Effect of temperature difference

Through the literature research, it is known that the heat recovery efficiency of C-TREC systems is mostly set at 70 %, Fig. 9(a) and Fig. 9(b) show the distribution of maximum power density and system efficiency of the continuous type TREC system under different temperature difference conditions, respectively. Equations (18), (21) and (22) show that as the temperature difference between the two cells increases, the voltage of the system will rise, thus increasing the power density of the system. The power density and efficiency of the system will also grow gradually as the temperature difference increases. This shows that the C-TREC system can be good in application scenarios where low and medium temperature heat.

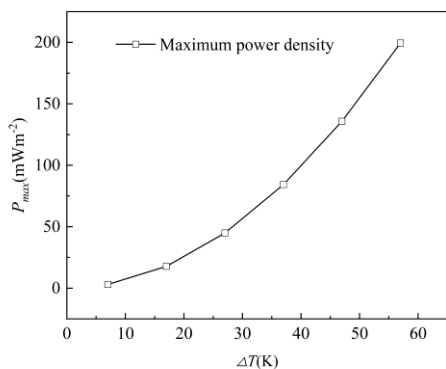


Fig. 9 (a) Maximum power density of C-TREC system for different temperature differences

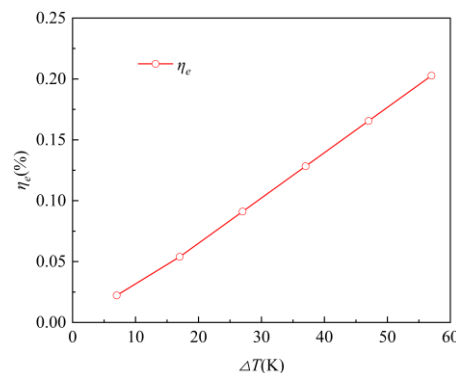


Fig. 9 (b) Efficiency of continuous TREC system with different temperature difference

## 4. CONCLUSION

In this study, a two-dimensional model of the mass transfer and reaction kinetics of the C-TREC taking into account the steady state is developed and validated. The effects of parameters such as current density, overpotential distribution, porous electrode geometry, temperature difference and the use of different electrolytes at the same flow rate on the performance of the system were analyzed. The conclusions are as follows:

(1) A two-dimensional steady-state continuous TREC model simulation modelling framework based on electrochemical reaction unit (ERU) charging and discharging strategies coupled with flow and electrochemical fields is established.

(2) Electrode geometry and porosity are important parameters affecting the performance of porous electrodes. Larger porosity enhances the mass transfer process and thus improves the performance of a continuous TREC, while reducing the electrode thickness also helps to improve the performance of the system.

(3) Larger current density produces a larger overpotential, which reduces the voltage of the system. Higher current densities increase the power density of the system, but the power density decreases gradually when the value of the current reaches a certain critical value. The flow field distribution is significantly affected by current density and electrolyte flow rate. The higher the current density, the higher the overpotential and the lower the system voltage. Increasing the temperature difference between two cells increases the maximum power density and efficiency of a continuous TREC system.

## ACKNOWLEDGEMENT

The authors declare that they have no known competing financial interests or personal relationships that could have appeared to influence the work reported in this paper. All authors read and approved the final manuscript.

## REFERENCE

- [1]Johnson I, Choate WT, Davidson A. Waste heat recovery. Technology and opportunities in US industry. Laurel, MD (United States): BCS, Inc.; 2008.
- [2]Mahmoudi A, Fazli M, Morad MR. A recent review of waste heat recovery by Organic Rankine Cycle. Applied Thermal Engineering. 2018; 143:660-675.
- [3]Dupontd MF, Macfarlane DR, Pringle JM. Thermo-electrochemical cells for waste heat harvesting – progress and perspectives[J]. Chemical Communications, 2017, 53(47): 6288-6302.
- [4]Dupontd MF, Macfarlane DR, Pringle JM. Thermo-electrochemical cells for waste heat harvesting – progress and perspectives[J]. Chemical Communications, 2017, 53(47): 6288-6302.
- [5]Lee SW, Yang Y, Lee H, Ghasemi H, Kraemer D, Chen G, et al. An electrochemical system for efficiently harvesting low-grade heat energy. Nature Communications, 2014, 5(1): 3942.
- [6]Zhang F, Liu J, Yang W, Logan BE. A thermally regenerative ammonia-based battery for efficient harvesting of low-grade thermal energy as electrical power. ENERG ENVIRON SCI. 2015; 8:343-349.
- [7]Yip NY, Vermaas DA, Nijmeijer K, Elimelech M. Thermodynamic, Energy Efficiency, and Power Density Analysis of Reverse Electrodialysis Power Generation with Natural Salinity Gradients. ENVIRON SCI TECHNOL. 2014; 48:4925-4936.
- [8]Facchinetti I, Ruffo R, La Mantia F, Brogioli D. Thermally Regenerable Redox Flow Battery for Exploiting Low-Temperature Heat Sources. Cell Reports Physical Science. 2020; 1:100056.
- [9]Abdollahipour A, Sayyaadi H. A review of thermally regenerative electrochemical systems for power generation and refrigeration applications. APPL THERM ENG. 2021; 187:116576.
- [10]Cheng C, Dai Y, Yu J, Liu C, Wang S, Feng SP, et al. Review of Liquid-Based Systems to Recover Low-Grade Waste Heat for Electrical Energy Generation. ENERG FUEL. 2021; 35:161-175.
- [11]Yang Y, Lee SW, Ghasemi H, Loomis J, Li X, Kraemer D, et al. Charging-free electrochemical system for harvesting low-grade thermal energy. Proceedings of the National Academy of Sciences. 2014; 111:17011-17016.
- [12]Poletayev AD, McKay IS, Chueh WC, Majumdar A. Continuous electrochemical heat engines. Energy & Environmental Science. 2018; 11:2964-2971.
- [13]Poletayev AD, McKay IS, Chueh WC, Majumdar A. Continuous electrochemical heat engines. Energy & Environmental Science. 2018; 11:2964-2971.
- [14]Zhang H, Zhang F, Yu J. Redox Targeting-Based Thermally Regenerative Electrochemical Cycle Flow Cell for Enhanced Low-Grade Heat Harnessing[J]. Advanced Materials, 2021, 33(5): 2006234.
- [15]Reynard D, Dennison Battistel A, Girault HH. Efficiency improvement of an all-vanadium redox flow battery by harvesting low-grade heat. J POWER SOURCES. 2018; 390:30-37.
- [16]Eapen DE, Choudhury SR, Rengaswamy R. Low grade heat recovery for power generation through electrochemical route: Vanadium Redox Flow Battery, a case study. APPL SURF SCI. 2019; 474:262-268.
- [17]Ding Y, Guo X, Ramirez-Meyers K, Zhou Y, Zhang L, Zhao F, et al. Simultaneous energy harvesting and storage via solar-driven regenerative electrochemical cycles. ENERG ENVIRON SCI. 2019; 12:3370-3379.
- [18]Qian X, Shin J, Tu Y, Zhang JH, Chen G. Thermally regenerative electrochemically cycled flow batteries with pH neutral electrolytes for harvesting low-grade heat. PHYS CHEM CHEM PHYS. 2021.
- [19]Bleeker J, Reichert S, Veerman J, Vermaas DA. Thermo-electrochemical redox flow cycle for continuous conversion of low-grade waste heat to power[J]. Scientific Reports, 2022, 12(1): 7993.
- [20]Li X, Li J, Yun J, Wu A, Gao C, Lee SW. Continuous thermally regenerative electrochemical systems for directly converting low-grade heat to electricity. Nano Energy 2022; 101:107547.
- [21]Chen R, Deng S, X Zhao L, et al. Progress and prospects for low-grade heat recovery electrochemical technologies. Sustain Energy Technol Assess 2022; 49:101802.
- [22]Ding Y, Guo X, Ramirez-Meyers K, Zhou Y, Zhang L, Zhao F, et al. Simultaneous energy harvesting and storage via solar-driven regenerative electrochemical cycles. Energy & Environmental Science, 2019, 12(11): 3370-3379.
- [23]Shah AA, Watt-Smith MJ, Walsh FC. A dynamic performance model for redox-flow batteries involving soluble species. Electrochimica Acta, 2008, 53(27): 8087-8100.

[24]Qian X, Shin J, Tu Y, Zhang JH, Chen G. Thermally regenerative electrochemically cycled flow batteries with pH neutral electrolytes for harvesting low-grade heat. *Physical Chemistry Chemical Physics* 2021; 23:22501–14.